Exploring a Nitrogen Vacancy Center Quantum Computer

Dillion Cottrill
Physics and Astronomy Department, SUNY Stony Brook
(Dated: December 19, 2022)

Quantum computing is a burgeoning subject. With its growth, many implementations to control qubits, which are commonly emobodied with two level quantum systems, have been proposed and implemented. Herein this report, I will describe several methods used to characterize a NV^- Diamond center, one of the most exciting methods for creating operable quantum computers. I will describe it's theory of operation, several examples of characterization, and finally give details on the implementation of a Pseudo Deutsch-Joza algorithm. I will first provide an introduction to the field of quantum computing and what is possible with these devices. Then, I will discuss fundamental theory of quantum information processing, as well as the physics required to operate the quantum computer. Finally, I will present the results of my experimentation on the quantum computer.

I. INTRODUCTION

A. Introduction To Quantum Computers

Qubits are perhaps the most fundamental element of quantum information theory, a subject which is concerned with the representation, computation, and transfer of information in the form of simple quantum systems. A qubit can be represented with an extremely simple quantum system, simply the coupling two energy levels. A qubit, much like a bit, has two states, 0 and 1, though with a "third" state described as a superposition state which can be thought of as a state with some probability of being 0, and some other complementary probability of the state being 1. It is described by the following equation:

$$|\psi\rangle = A\,|0\rangle + B\,|1\rangle \tag{1}$$

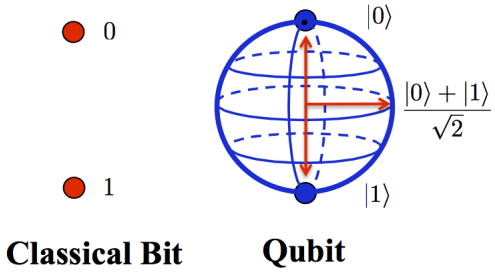

FIG. 1. Bit representation next to qubit. The state on the right is an equal superposition of 1 and 0.Credit to CIQTEK.

In order for quantum computers to become useful and become integrated into our daily lives, they must satisfy the David DiVincenzo Criteria, set in place in 2000. This consists of 7 criteria:

1. Scalable Systems of qubits with fully described qubits.
2. Initialization of qubit
3. Decoherence times which enable operation
4. A universal set of quantum gates
5. Ability to measure and readout specific qubits
6. high fidelity transduction between flying and computational qubits
7. high fidelity flying qubtis

The work within this report will discuss a few of these items, namely criterion 2,3, and 5.

B. Quantum Logic Gates

Once a quantum computer has the basic elements necessary to support qubits, gate operations may then be designed and implemented. Here we will discuss criteria 4, a universal set of quantum gates.

A universal set of quantum gates enables all possible operations on quantum states to be implemented[1]. This means that, for example, some initialized state can be prepared into a superposition, or that with some subset of gates, all other operations are implementable. An example of a set of universal gates is the CNOT, S, H, and T gates, which together can be described as the Clifford and T gate. Another set is the Toffoli and Hadamard gates. All gates can be represented by $2^n \times 2^n$ matrices. Figure 2 displays some common gates.[2]

C. Usefulness of Quantum Computing

Quantum computing algorithms have several significant advantages over classical computers, due to several ingenous algorithms which have been created over the years. The one which perhaps has the most media coverage is Shor's algorithm, which states that quantum computers can factor large prime numbers faster than their classical counterparts. This is concerning and has garnered significant attention from the media due to RSA encryption, which itself is based on the security of large prime number factorization. With quantum computers, the possibility of hacking is a real worry.[4]

Gate	Equation	Matrix	Transform	Notation
Identity (*I*)	$I = \|0\rangle\langle 0\| + \|1\rangle\langle 1\|$	$\begin{pmatrix} 1 & 0 \\ 0 & 1 \end{pmatrix}$	$I\|0\rangle = \|0\rangle$ $I\|1\rangle = \|1\rangle$	I
Pauli-*X* (*X* or **NOT**)	$X = \|0\rangle\langle 1\| + \|1\rangle\langle 0\|$	$\begin{pmatrix} 0 & 1 \\ 1 & 0 \end{pmatrix}$	$X\|0\rangle = \|1\rangle$ $X\|1\rangle = \|0\rangle$	X
Hadamard (*H*)	$H = \frac{\|0\rangle+\|1\rangle}{\sqrt{2}}\langle 0\| + \frac{\|0\rangle-\|1\rangle}{\sqrt{2}}\langle 1\|$	$\frac{1}{\sqrt{2}}\begin{pmatrix} 1 & 1 \\ 1 & -1 \end{pmatrix}$	$H\|0\rangle = \frac{1}{\sqrt{2}}(\|0\rangle+\|1\rangle)$ $H\|1\rangle = \frac{1}{\sqrt{2}}(\|0\rangle-\|1\rangle)$	H
Controlled-NOT (**CNOT**)	$\mathbf{CNOT} = \|0\rangle\langle 0\| \otimes I + \|1\rangle\langle 1\| \otimes X$	$\begin{pmatrix} 1 & 0 & 0 & 0 \\ 0 & 1 & 0 & 0 \\ 0 & 0 & 0 & 1 \\ 0 & 0 & 1 & 0 \end{pmatrix}$	$\mathbf{CNOT}\|00\rangle = \|00\rangle$ $\mathbf{CNOT}\|01\rangle = \|01\rangle$ $\mathbf{CNOT}\|10\rangle = \|11\rangle$ $\mathbf{CNOT}\|11\rangle = \|10\rangle$	
Toffoli (*T* or **CCNOT**)	$\mathbf{T} = \|0\rangle\langle 0\| \otimes I \otimes I + \|1\rangle\langle 1\| \otimes \mathbf{CNOT}$	$\begin{pmatrix} 1&0&0&0&0&0&0&0 \\ 0&1&0&0&0&0&0&0 \\ 0&0&1&0&0&0&0&0 \\ 0&0&0&1&0&0&0&0 \\ 0&0&0&0&1&0&0&0 \\ 0&0&0&0&0&1&0&0 \\ 0&0&0&0&0&0&0&1 \\ 0&0&0&0&0&0&1&0 \end{pmatrix}$	$\mathbf{T}\|000\rangle = \|000\rangle, \mathbf{T}\|001\rangle = \|001\rangle$ $\mathbf{T}\|010\rangle = \|010\rangle, \mathbf{T}\|011\rangle = \|011\rangle$ $\mathbf{T}\|100\rangle = \|100\rangle, \mathbf{T}\|101\rangle = \|101\rangle$ $\mathbf{T}\|110\rangle = \|111\rangle, \mathbf{T}\|111\rangle = \|110\rangle$	

FIG. 2. Some common quantum computing operations. Credits: [3].

Another significant find is Grover's search algorithm, which can sort a list quadratically faster than the best classical algorithm. This would be particularly advantageous for fields like data science, and useful anyone dealing with extremely large data sets like Google, Facebook, or Youtube.

These are but a taste of the power of quantum algorithms. We won't implement any of these algorithms within this report, but we will discuss the Deutsch-Joza algorithm, though it has little commercial value as it stands today.

II. THEORY

A. NV Centers

A nitrogen vacancy center can be thought of as a defect in the conventional carbon lattice of a diamond. Instead of an atom of carbon with 6 valence electrons,it has been replaced it with a nitrogen atom, with only 5 valence electrons. Then, another carbon atom is removed, and a vacancy is left in the lattice. This pair within the lattice, often referred to as the NV center, is negatively charged, and has a unique energy structure from the other parts of the crystal. [5]

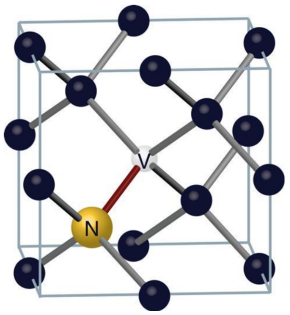

FIG. 3. A diagram of an NV Center. Credits for illustration go to Peter Allen

One of the greatest strengths of the NV center is room temperature operation. While at room temperature, we have access to a sophisticated assortment of energy levels, namely a ground state triplet state, excited state triplet, and two intermediate state singlets. This is illustrated in figure 4.

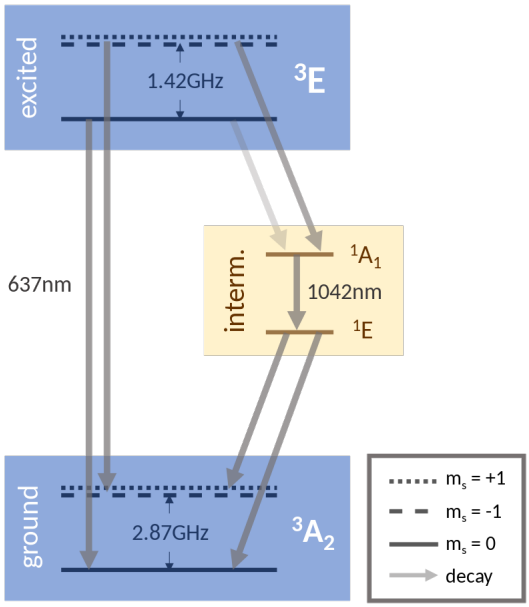

FIG. 4. Energy level diagram of an NV diamond center.

When there is no magnetic field in place, the $|M_s = 1\rangle$ and $|M_s = -1\rangle$ are degenerate, with a difference of 2.87GHz between the degenerate state and the $|M_s = 0\rangle$ state. Likewise, the excited triplet $|M_s = \pm 1\rangle$ states are degenerate and have a seperation of 1.42GHz from the $|M_s = 0\rangle$ state. In our system, a 520nm laser is used to send electrons from the respective energy levels to the spin-conserving levels in the excited states. This means that the spin stays the same, and so the electrons in $|M_s = 0\rangle$ go to the excited $|M_s = 0\rangle$ state, and the ground state $|M_s = \pm 1\rangle$ go to the excited state $|M_s = \pm 1\rangle$ levels. Many of the cycles will cause immediate radiative decay, though as you can see by figure 4, some of the $|M_s = \pm 1\rangle$ states will go through the non-

radiative transition via phonon coupling.

The key element here is that by the non-radiative transitioning of $|M_s = \pm 1\rangle$, we will effectively pump electrons into the $|M_s = 0\rangle$ ground state, effectively inducing a polarization of the NV center. In the QC manual, polarization of up to 95% is possible.

We can now assume that the ground states $|M_s = 0\rangle$ and $|M_s = 1\rangle$ can be treated as the qubit. Because of the conservation of spin via the transitions, the polarization of the vacancy center is dependent on the initial state of the qubit. By using the fluorescence intensity of the transitions, we can determine the state which the electron is in. The $|M_s = 0\rangle$ state is around 30% brighter than the other two transitions, and using this feature, readout is achieved.[6]

B. Spin Procession

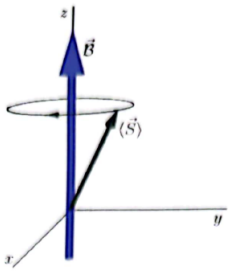

FIG. 5. Geometric illustration of Spin or Larmor procession.

To manipulate the state of our qubit, we will implement a spin-magnetic resonance technique using a microwave field. We must first describe the Hamiltonian of our system, as well as define the relationship of the magnetic field to the spin. Using $H = \overrightarrow{-\mu} \cdot \overrightarrow{B_0}$ where $\overrightarrow{\mu} = \gamma \overrightarrow{S}$, the Hamiltonian becomes:

$$H = \frac{\hbar}{2} \begin{pmatrix} \gamma B_0 & 0 \\ 0 & -\gamma B_0 \end{pmatrix} = \frac{\hbar}{2} \begin{pmatrix} \omega_0 & 0 \\ 0 & -\omega_0 \end{pmatrix} \tag{2}$$

Here, γ is the gyromagnetic ratio, ω_0 is the frequency of the photon, B_0 is a static magnetic field, and $\overrightarrow{S}$ is the spin operator. We are now interested in determining how an arbitrary state changes with time. To do so we plug this Hamiltonian into the Schrodinger equation:

$$i\hbar \begin{pmatrix} \dot{a} \\ \dot{b} \end{pmatrix} = -\frac{\hbar}{2} \begin{pmatrix} \omega_0 & 0 \\ 0 & -\omega_0 \end{pmatrix} \begin{pmatrix} a \\ b \end{pmatrix} \tag{3}$$

Which when solved yield solutions which are exponential. The spin expectation values are then:

$$\langle S_z \rangle = \frac{\hbar}{2} Cos(\alpha) \tag{4}$$

$$\langle S_x \rangle = \frac{\hbar}{2} Sin(\alpha) Cos(\omega_0 t + \alpha_0) \tag{5}$$

$$\langle S_y \rangle = -\frac{\hbar}{2} Sin(\alpha) Sin(\omega_0 t + \alpha_0) \tag{6}$$

These equations describe the spin procession the electron follows in a constant magnetic field. ω_0 is the Larmor frequency. Figure 5 is a good example of the procession of the magnetic moment of the electron.

C. Microwave Resonance

Rabi oscillations can be realized due to a driving external magnetic field with frequency that matches the Larmor frequency. This process is key, as this is the method which we will use to coherently manipulate the spin qubit. The physical process of the Rabi oscillation is simple: the qubit is effectively oscillating around the Bloch sphere, and by timing our pulses carefully, we can effectively manipulate our qubits position in the Bloch sphere.[7]

This is accomplished by using a circularly polarized microwave field with components of polarization in the x and y axis, and propgating in the z direction, with components $B_x = B_1 Cos(\omega t)$ and $B_y = B_1 Sin(\omega t)$. Using $\omega_1 = \gamma B_1$ and substituting into the Schrodinger equation as before, we can solve for the term a. Assuming we are in the state $\Psi(0) \equiv |1\rangle$, we can show that the probability of spin up as a function of time is:

$$P_\uparrow = |a(t)|^2 = \frac{\omega_1^2}{\delta^2} Sin^2(\delta t) \tag{7}$$

Where $\delta = \sqrt{\omega_1^2 + (\omega_0 - \omega)^2}$.

This process of introducing a secondary magnetic field causes a motion described geometrically with the Bloch sphere in figure 6.

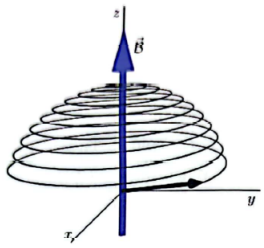

FIG. 6. Geometric illustration of rabi oscillation.

When $\omega_1 t = \pi$ of the magnetic field, via a pulse, we can create a bit flip, referred to as a NOT gate. When $\omega_1 t = \frac{\pi}{2}$, we will have effectively implemented a Hadamard transform, where an equal superposition is achieved.

We can see now that by shaping our pulses, we are able to manipulate the state of the qubit, and perhaps implement more sophisticated gates and operations on our two level system.

III. EXPERIMENTS

A. Overview of Device Control

There are four modules within the CIQTEK Quantum Computer: Microwave Module, Power Module, Control and Acquisition Module, and the Optical Module. These modules are connected in various ways, though the heart of the device is certainly the optical module, where the diamond is held.

The optical module holds the pulse laser generator, optical cage system, microwave radiation structure, the diamond, and a photodetector. The laser generator creates the pulses of 520nm light which we use to initialize and readout the qubit. The optical cage system supports the various optical elements necessary, such as lenses and polarizers. A photodetector is at the end of the optical cage system, and converts the fluorescence to electrical signals. These signals are then sent to other modules.

The Microwave module generates the bursts of microwaves necessary to perform manipulation on the qubit.

The control and acquisition module regulates the pulses, and also receives the the information from the optical module from the photodetector. This module is where orchestration of all devices within the device is done, which includes synchronization, pulsing, detecting, and displaying information.

The power module provides the necessary energy drawn by the rest of the device, and has a working voltage of 110 240 V, 50/60Hz AC and a current of .6 Amps.

B. Characterization

The first step in using this device is the characterization of the NV center. We do so by scanning the microwave frequency, while changing the magnetic field. Through this methodology, we perform spectroscopy on our diamond sample, and in the process determine the splitting via the Zeeman effect due to the static magnetic field. Presented here is the experimental results of varying the distance of the magnet to the NV center from 0cm to 6cm. I found the most optimal distance was 4cm. For each of the trials, we obtained 5 sets of data. Here, we will only include the data from the 4cm trials, which we use for the remainder of the experiments. The others can be found in the appendix.

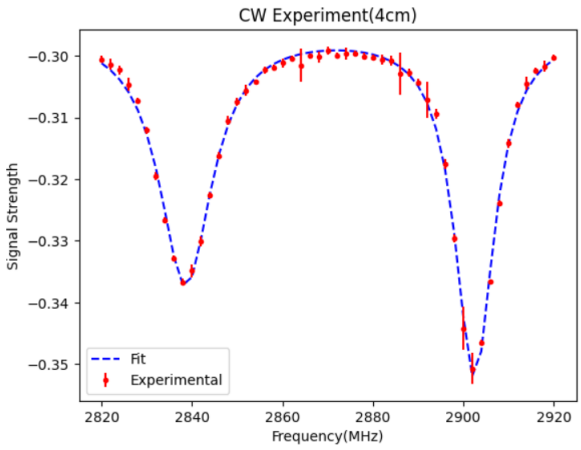

FIG. 7. Experimental data of CW spectroscopy of NV center.

Here it is clear to see the $|M_s = 0\rangle$ and $|M_s = 1\rangle$ states. We extract values 2838.6MHz and 2902.5MHz, which we use in later experiments.

C. Rabi Oscillation

The key element in determining the 2π,π, and $\pi/2$ pulse is the fitting of Rabi Oscillation. Here, we provide a fitting of the observed oscillations. We obtain the values 73ns, 36ns, and 146ns for the $\pi, \frac{\pi}{2}$, and 2π pulses respectively via the best fit.

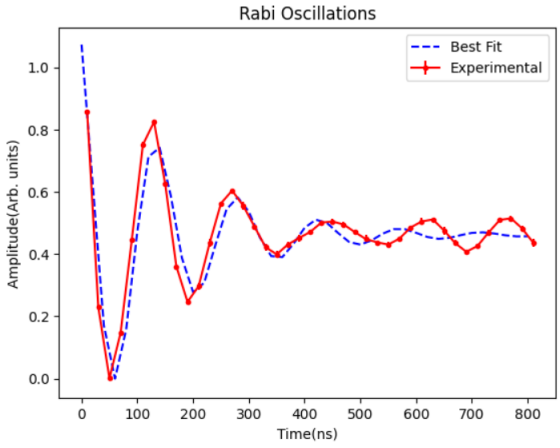

FIG. 8. Experimental data of the Rabi Oscillations observed at a magnet placement of 4cm.

Note that near the end of the Rabi Oscillation, the tail perhaps exhibits driven oscillation. This may be due to a mismatch in the frequencies. The Rabi oscillations occur between the states $|M_s = 0\rangle$ and $|M_s = 1\rangle$, and describe the length of pulse needed to flip the qubit or to initialize it into a superposition. The Rabi Oscillation allows us to also create an arbitrary superposition state, assuming no decoherence.

D. Hahn Spin Echo

The goal of the Echo experiment is to use pulses to recohere a state which has become decoherent. The process begins with the initialization of the qubit to a $|0\rangle$ state. Then the system is prepared into an equal superposition $\frac{1}{\sqrt{2}}(|0\rangle + |1\rangle)$ using a $\frac{\pi}{2}$ pulse and the system is allowed to evolve in time. Then, sometime t1 later, a π pulse is applied. We wait some time $t \neq t1$, and then we send another $\frac{\pi}{2}$ pulse, which refocuses the noise of the spin, essentially removing inhomogenous dephasing. After some time Here we show the results of the experiment.[8]

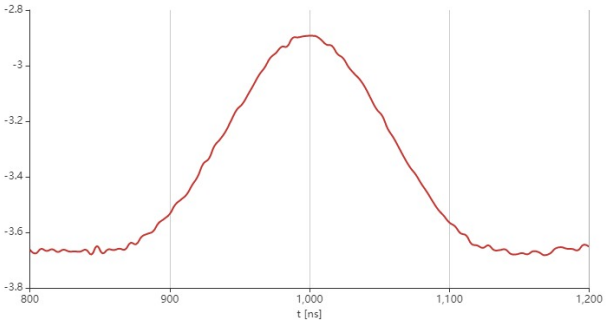

FIG. 9. Data on Hahn Spin Echo. The y-axis is amplitude, and the x axis is time.

The process of the Spin Echo is an important component of modern nuclear medicine, and is utilized in MRIs. The interesting component of this module is the echo signal which is received after the pulses, illustrated in figure 9. As expected, this shape is Gaussian.

E. T2

Primarily to measure the coherence time of the NV center, this experiment is a simple method of measuring the rate at which the environment begins to effect the spin qubit. The pulse timing is similar to that of the Spin echo, with the caveat that the time between initialization and readout are the same, $\tau = \frac{t}{2}$, though we instead hope to measure the decoherence timescale rather than detect the spin echo. Both the T2 and the Spin Echo pulse sequence is included in the Appendix.

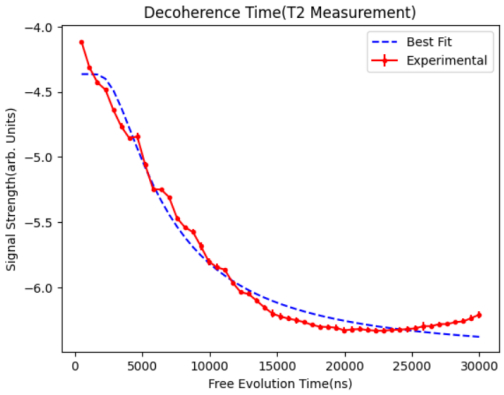

FIG. 10. Data on decoherence time, T2.

This is often referred to as the Ramsey Experiment, and measures the decay time T2. This value is approximately 5562 nanoseconds.

F. Dynamic Decoupling

By carefully choosing our pulse operation sequence, we can effectively suppress decoherence inherent to a quantum system coupled to an external environment. This method takes advantage of the average Hamiltonian method, where essentially the environmental effects are averaged out over time.

This experiment is often referred to as the Free Induction Decay experiment, or $T2^*$. With, we hope to increase the coherence time to near infinity for our initialized state.

Our data agrees with theoretical predictions, with some leveling off of the probability of achieving our state. The Y axis here should be normalized to 1, and predicts the probability of our qubit being in the initialized state. The X axis is the time in nanoseconds. Ideally, the decoherence time T2 is lengthened to infinity.

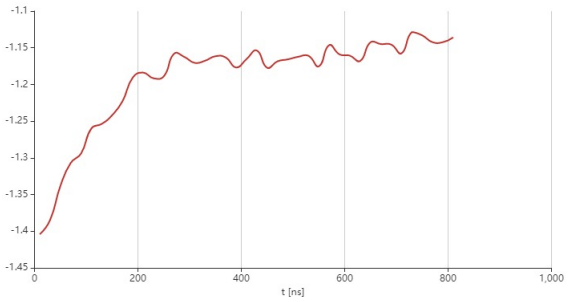

FIG. 11. Dynamic Decoupling.

The pulse sequence is identical to that of the T2 data, with the exception that we repeat the pi pulses M times, and shorten the time betwween pulses to $\frac{t}{2M}$.

G. Deutsch-Joza Algorithm

The function if the Deutsch-Joza algorithm is to determine whether a function f(x) is constant or balanced. A constant function outputs the same bit-wise value regardless of the argument x, while a balanced function has an equal output of 0 and 1.

We define a unitary operation$U_f(x) = (-1)^{f(x)}|x\rangle$ which f(x) can be one of four functions which are constant or balanced. The functions are f1(x)=0, f2(x)=1, f3(x)=x, f4(x)=1-x. The balanced fuctions f1 and f2 can be represented as the 2x2 identity matrix, either positive or negatively valued respectively. f3 and f4 are the Pauli Z matrix, also positive or negative respectively. We begin with an initialization of our qubit, then a Hadamard transform via a $\frac{\pi}{2}$ pulse. Then, four combinations of $2pi$ pulses are used to implement the U_f gates. Depending on the type of function we input, we will see an equal superposition. If it is constant, we will see:

$$\pm\frac{|0\rangle + |1\rangle}{\sqrt{2}} \tag{8}$$

If the function is balanced we will have:

$$\pm\frac{|0\rangle - |1\rangle}{\sqrt{2}} \tag{9}$$

these values directly correspond to a forward or reverse echo, and thus the echos are used to determine the function behavior. Below I have attached my experimental outcome for the four different functions described above.

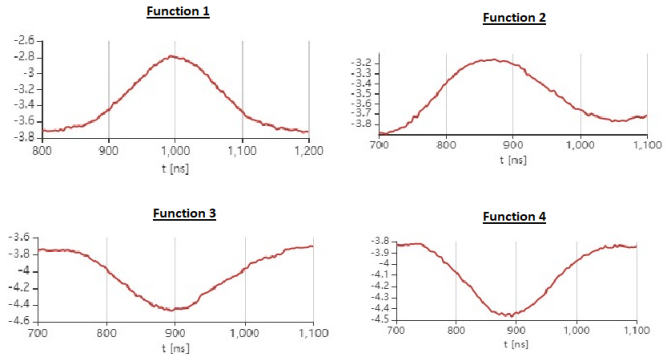

FIG. 12. Results of Deutsch Joza Algorithm. from left to right(Top) function 1, function 2. (Bottom) function 3, function4.

Here, from the shape of the gaussian we can determine whether this is a positive or negative spin echo.

IV. CONCLUSIONS

NV^- centers are a diverse and promising area of quantum computing hardware, and from these experiments, it is clear that there is significant progress being made towards public access to quantum computers. From these activities, it is clear that we have coherent control over a spin qubit, which can be characterized, initialized, manipulated, and even used to implement the Deutsch Joza algorithm.

ACKNOWLEDGMENTS

I would like to thank Leonardo Castillo-Veneros For assistance and guidance in taking the data for the first two modules of the quantum computing experiment. I would like to thank Dounan Du for advice on how to fit the error bars.

V. APPENDIX

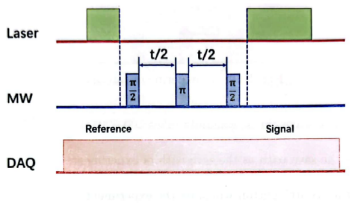

FIG. 13. T2 pulse sequence.

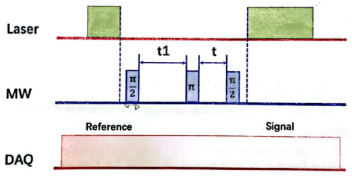

FIG. 14. Echo pulse sequence.

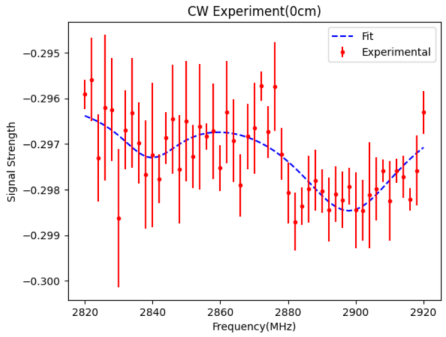

FIG. 15. 0cm from NV center magnet positioning fit.

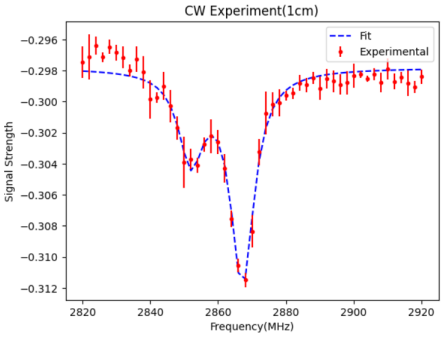

FIG. 16. 1cm from NV center magnet positioning fit.

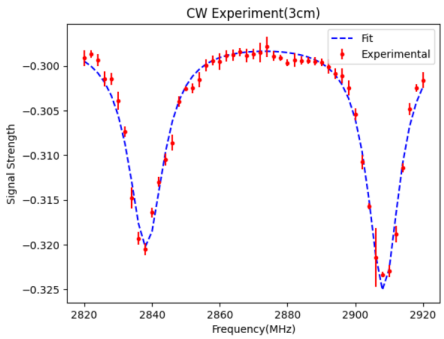

FIG. 18. 3cm from NV center magnet positioning fit.

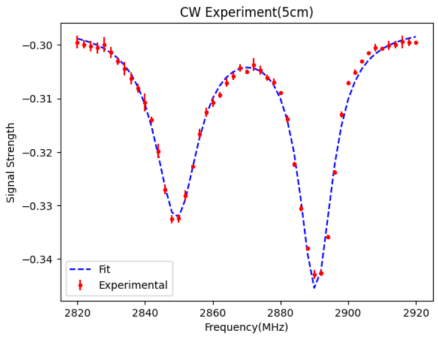

FIG. 19. 5cm from NV center magnet positioning fit.

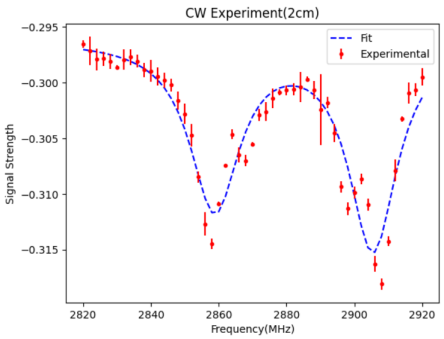

FIG. 17. 2cm from NV center magnet positioning fit.

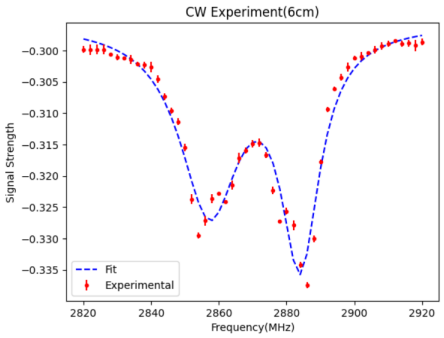

FIG. 20. 6cm from NV center magnet positioning fit.

[1] A. Barenco, C. H. Bennett, R. Cleve, D. P. DiVincenzo, N. Margolus, P. Shor, T. Sleator, J. A. Smolin, and H. Weinfurter, Elementary gates for quantum computation, Phys. Rev. A **52**, 3457 (1995).

[2] C. P. Williams, Quantum gates, in *Explorations in Quantum Computing* (Springer London, London, 2011) pp. 51–122.

[3] F. Yan, A. Iliyasu, and K. Hirota, Conceptual framework for quantum affective computing and its use in fusion of multi-robot emotions, Electronics **10**, 100 (2021).

[4] IBMQ, *Qiskit* (IBM Quantum, 2021).

[5] S. B. University, *Quantum Computing Write Up* (Stony Brook University, 2021).

[6] CIQTEK, *Quantum Computing Manual* (CIQTEK, 2020).

[7] R. Fitzpatrick, (2020), Physics Libre Texts 9.5 Spin Precession.

[8] N. B. Manson, J. P. Harrison, and M. J. Sellars, Nitrogen-vacancy center in diamond: Model of the electronic structure and associated dynamics, Phys. Rev. B **74**, 104303 (2006).

[9] D. Aharonov, A simple proof that toffoli and hadamard are quantum universal (2003).

[10] P. Shor, Algorithms for quantum computation: discrete logarithms and factoring, in *Proceedings 35th Annual Symposium on Foundations of Computer Science* (1994) pp. 124–134.